

Indentation Fracture Toughness Measurement and Application to Low-K Thin Film

Huai Huang

Materials Laboratory for Interconnect and Packing, PRC/MER, Austin, Texas, 78712-1100

ABSTRACT

As the thickness of coating thin film is reduced it becomes increasingly difficult to measure their adhesion, hardness, toughness by conventional methods. Indentation test methods are well established for the determination of elastic modulus and hardness, but methods for assessment of fracture properties are much less developed. In this term paper, existing metrology of using indentation to study fracture toughness will be summarized and mechanics of fracture under indentation will be studied. Experimental plans of investigation fracture toughness of OSG low-K film will also be evaluated in the end.

INTRODUCTION

Nanoindentation is widely used as an important tool for measuring the mechanical properties of thin films. Ordinary indentation hardness testing involves forcing a sharp indenter (usually diamond) into the surface of a solid with a fixed load or force and then measuring the projected area of the impression left in the surface (Fig. 1 (a)). With this testing methodology, the hardness is usually defined as

$$H = \frac{\text{Load}}{\text{Area}} = \frac{P}{A} \quad (1)$$

where the load P is the maximum load applied and the area A is the projected area of the resulting impression.

Nanoindentation involves forcing a sharp diamond indenter into the surface of a thin film on a substrate, while measuring the force imposed and the corresponding displacement of the indenter. Thus, nanoindentation is called a depth-sensing indentation technique. The principal resolution figures are: for load resolution is around $0.25\mu\text{N}$, for displacement resolution is 0.3nm and for position resolution $\sim 1\mu\text{m}$, which is sufficient to obtain useful mechanical property data for films as thin as about 100 nm .

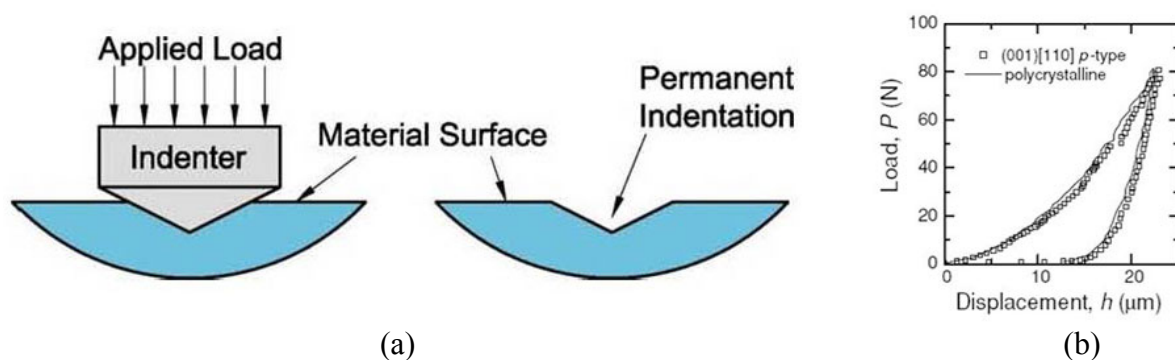


Figure 1. (a) Schematic illustration of a nanoindentation test; (b) A load and displacement curve obtained by nanoindentation on silicon.

Nanoindentation has been widely used to characterize elastic properties such as the modulus, E , plastic properties such as the hardness, H , and time dependent properties [1]. However, the measurement of properties in fracture by indentation especially on thin film under $1\mu\text{m}$ was not well developed.

The fracture toughness of a material is a measure of its resistance to propagation of cracks. It typically measured by crack length c and applied load P it subjected to. For such a specimen, the stresses around the crack tip are given by

$$\sigma_{ij} = \frac{K}{\sqrt{2\pi r}} f_{ij}(\theta) \quad (2)$$

where r and θ are polar coordinates relative to the crack tip. The stress intensity factor, K ,

$$K = \beta P \sqrt{c} \quad (3)$$

where β is the geometry factor. The fracture toughness K_c is defined as the stress intensity factor of critical load needed to propagate the crack.

INDENTATION CRACKING

An understanding of the indentation fracture starts with a knowledge of the contact stress field. Such fields are determined principally by geometrical facts (indenter shape and material properties (elastic modulus, hardness and toughness).

Indentations can be classified as ‘sharp’ or ‘blunt’, depending on whether or not there is irreversible deformation at contact.

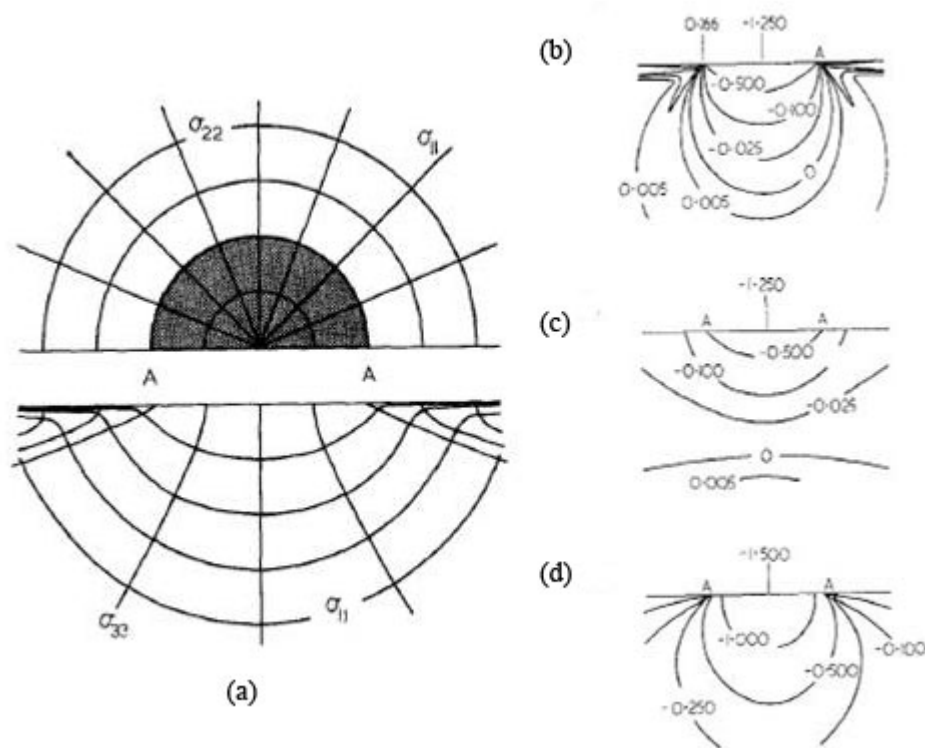


Figure 2. (a) Half-surface view (top) and side view (bottom) of stress trajectories in Hertzian field. (b)-(d) Contours of principal normal stresses, σ_{11} , σ_{22} and σ_{33} respectively. [2]

For ‘blunt’ indent, we could consider an isotropic, linear elastic half-space subjected to normal loading by a smooth spherical indenter. The original Hertz analysis gave explicit

quantitative consideration and in 1904 Huber extended the Hertz analysis and produced complete stress field solutions [2]

$$\frac{\sigma_{ij}}{p_0} = \left[g_{ij} \left(\frac{\rho}{a}, \frac{z}{a} \right) \right]_v \quad (4)$$

Stress field is illustrated in Figure 2. And the contact pressure:

$$P_0 = \frac{P}{\pi a^2} \quad (5)$$

Recalling the tendency for brittle cracks to propagate along paths normal to the greatest tensile stresses, we may predict the crack development as the classical Hertzian cone crack. The crack evolution are depicted schematically in figure 3(a): (i) pre-present surface flaws are subjected to tensile stresses outside the contact zone; (ii) at some point in the loading a favorably located flaw runs around the contact circle to form a surface 'ring' crack; (iii) on further loading, the embryonic ring crack grows incrementally down ward in the rapidly weakening tensile field; (iv) at critical load the ring becomes unstable and propagates down ward into the full frustum of the Hertzian cone (pop-in); (v) at still further loading the cone continues in stable growth (unless the contact circle expands beyond the surface ring crack, in which case the cone is engulfed on the compressive contact zone); (vi) on unloading, the crack closes.

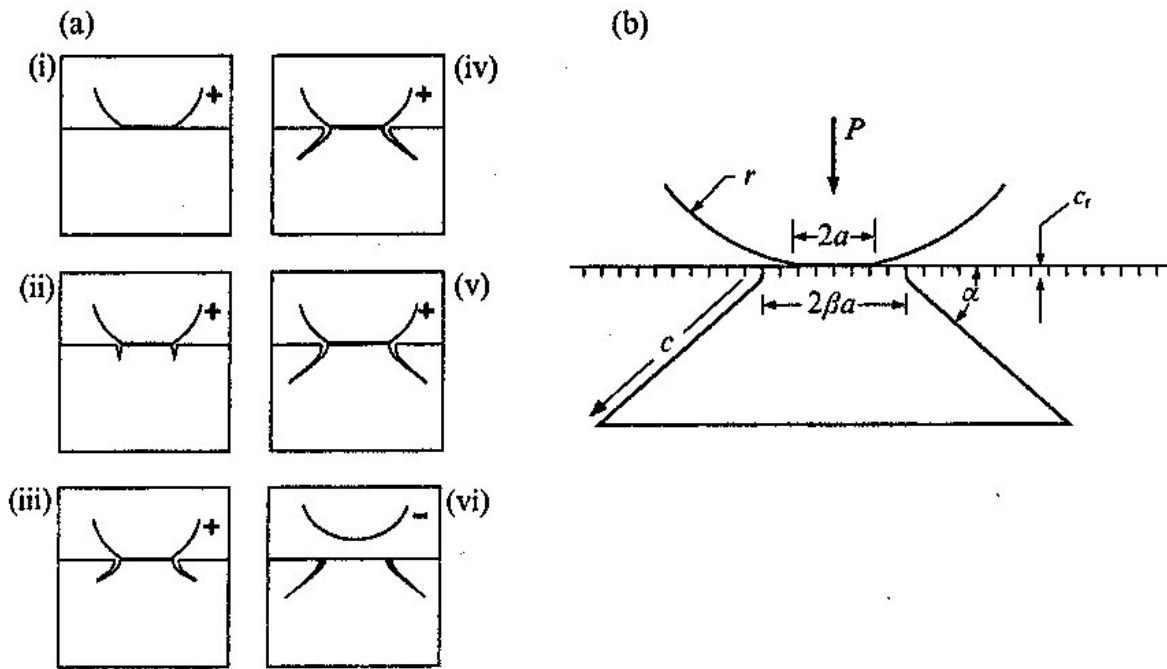


Figure 3. Hertzian cone crack system. (a) Evolution of cone during complete loading (+) and unloading (-) cycle. (b) Geometrical parameters

For 'sharp' indentation, we could consider an isotropic, linear elastic half-space subjected to a normal point load P . The solutions for the stress field in this configuration were first given by Boussinesq in 1885 [2][3]. The form is simple:

$$\sigma_{ij} = \left(\frac{P}{\pi R^2}\right)[f_{ij}(\phi)]_v \quad (6)$$

Stress field is illustrated in Figure 4. And the contact pressure:

$$P_0 = \frac{P}{\alpha_0 a^2} = H \quad (7)$$

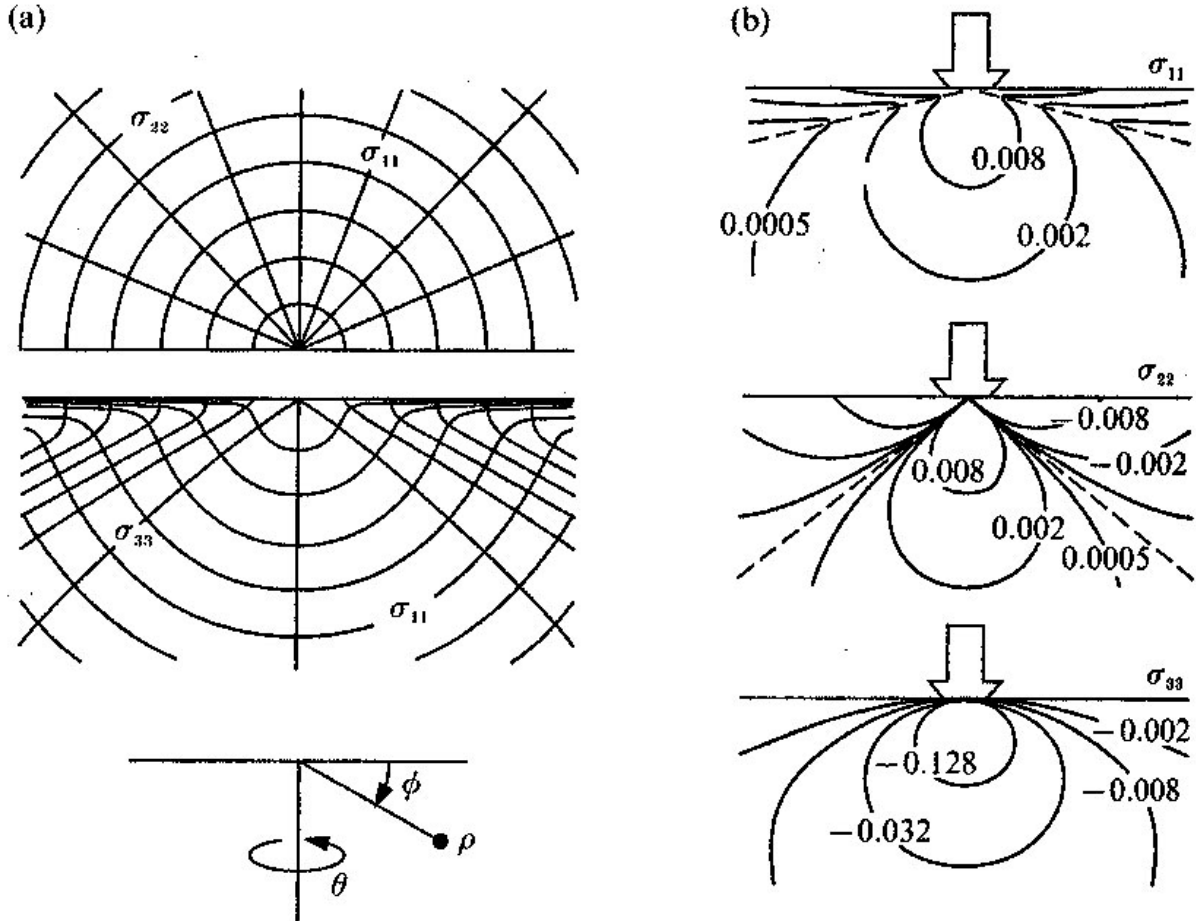


Figure 4. Boussinesq field. (a) Stress trajectories, half-surface view (top) and side view (bottom). (b) Contours, side view of σ_{11} , σ_{22} and σ_{33} respectively. [3]

In sharp-point limit, the deformation beneath the indenter point is irreversible until the contact is large enough to support the load. Sharp indenters like the Vickers or Knoop diamond pyramids used in hardness testing produce two basic types of crack pattern: radial-median and lateral. Figure 5(a) depicts the evolution of these crack systems: (i) the sharp point induces inelastic, irreversible deformation; (ii) at a critical load one or more nascent flaws within the deformation zone became unstable, and pop-in to form subsurface radial crack on tensile median planes, i.e. plans containing the load axis; (iii) on increased loading, the crack propagate incrementally downward; (iv) on unloading, the median crack close up below the surface as the contact recovers its elastic component; (v) just prior to removal of the indenter, the residual field becomes dominant, further expanding the surface radials and initiating a second system of sideways spreading near the base of the deformation zone; (vi) the expansion continues until

indenter removal is complete, both crack systems ultimately tending to half-pennies centred about the load point.

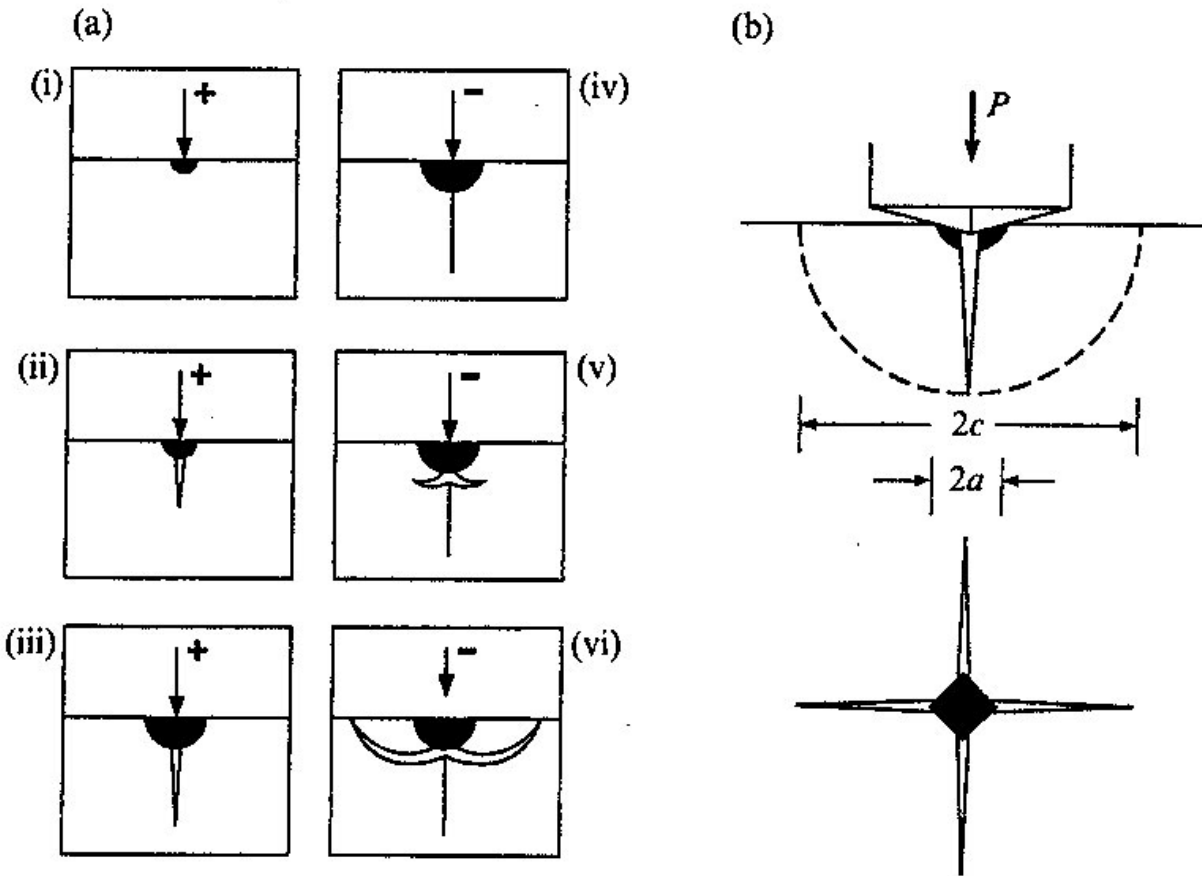


Figure 5. Radial-median and lateral crack systems. (a) Evolution during complete loading (+) and unloading (-) cycle. Dark region denotes irreversible deformation zone. (b) Geometrical parameters of radial system. [3]

FRACTURE MECHANICS ANALYSIS

An appropriate stress-intensity factor for the Hertzian cone crack system or the ideal radial-median configuration can both be written down from for centre-loaded penny-like cracks (figure 6) (the cone crack propagates on an ever-expanding circular front, we can simply regard the configuration as a centre-loaded):

$$K = \chi \frac{P}{c^{3/2}}, \quad (P > P_c, c \gg a) \quad (8)$$

The parameters c and a were defined in figure 3(b) and 5(b). The relations were also observed experimentally as figure 7. The quantity χ for cone cracks depends on Poisson's ratio, $\chi = \chi(\nu)$, [2][3] and is therefore a material constant. However, exact calculations of χ are not readily available, and one usually calibrates this term empirically from fits to data in figure 7(a). So fracture toughness measurement by blunt contact is not easy. The physical significance of χ for sharp-contact is totally different, which can be analytically given as [2][3][4]

$$\chi = \xi_0 (\cot \Phi)^3 \left(\frac{E}{H}\right)^{\frac{1}{2}} \quad (9)$$

with Φ the indenter half-angle. The dimensionless constant ξ_0 in this relation depends on the nature of the deformation. H is the hardness of the material which was defined in Eqn. (7). E is the modulus of the material.

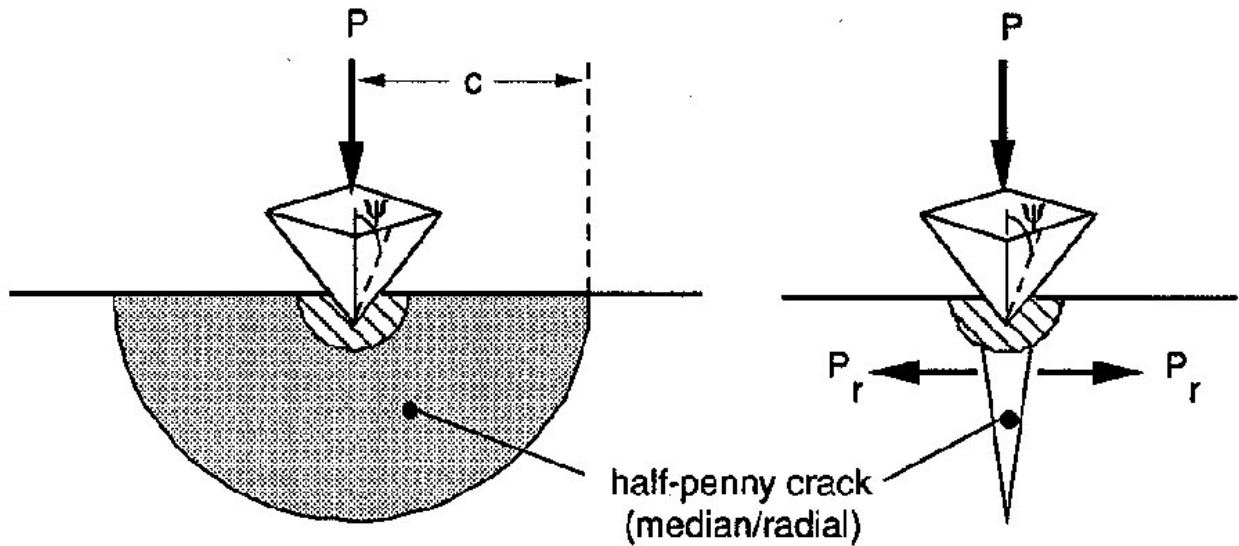


Figure 6. Geometry and loading parameters used in fracture mechanics analysis. [4]

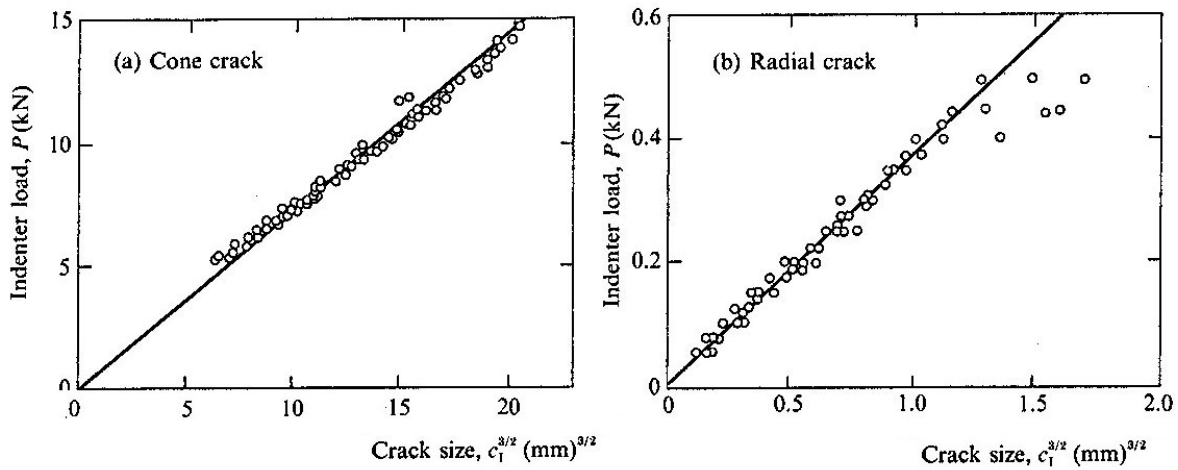


Figure 7. Indentation load vs characteristic crack size for (a) cone cracks (spherical indenter with machined flat) and (b) radial cracks (Vickers indenter) in soda-lime glass, inert environment. [3]

Combining Eqns. (8) and (9) and assuming that the crack arrests when it grows to a length at which the stress intensity factor is just equal to the fracture toughness, one obtains

$$K_c = \alpha \left(\frac{E}{H} \right)^{\frac{1}{2}} \left(\frac{P}{c^{\frac{3}{2}}} \right) \quad (10)$$

where α is an empirical constant depending on the geometry of the indenter, for example $\alpha=0.016$ for Vickers and Berkovich indenter and $\alpha=0.0319$ for cube corner indenter [4].

Basically, by measuring c and a in figure 5(b), the fracture toughness of the material can be subtracted from Eqn. (7) and (10). It is extreme simplicity and economy, many indentations can perform on one surface. But due to reasons like crack size definition and measurement, the accuracy of this method is within about 40%. [4] Indentation-strength measurement which measure inert strength as a function of indentation load by Eqn.(3) and (8) can be used as a alternate way.

APPLICATION TO THIN FILM

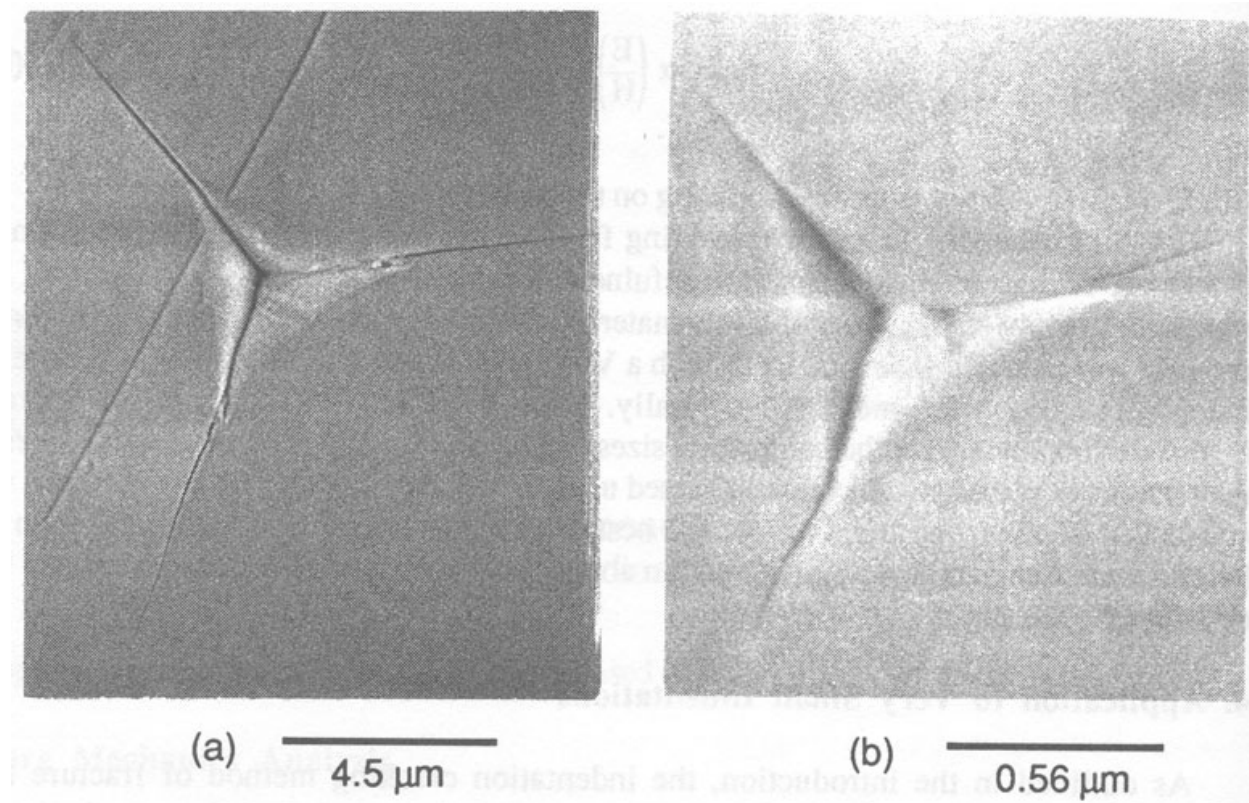


Figure 8. Indentations in fused quartz made with the cube corner indenter showing radial cracking. Indentation loads of (a) 12 grams and (b) 0.45 grams. [4]

The indentation cracking method of fracture toughness determination has been applied to indentations which are fairly large. The indentations are typically produced at loads of 1000 grams or greater, and the cracks are of the order of 100 μm in length. Since the size of the cracks sets a limit on the spatial resolution of the technique, much smaller indentations are needed for the test of thin film or small structure. For this purpose, smaller cracking thresholds (critical cracking load) are needed. G. M. Pharr et al. [4] found that lower cracking thresholds can be achieved by using sharper indenters and successfully reduced the critical load of fused quartz from 25gms to

around 0.5gms by replacing Vickers indenter to cube corner indenter. Thus crack length would be less than 1 μm , making the fracture toughness of much thinner films measurable (figure 8).

To test the applicability of Eqn.(10), Crack lengths for cube corner indenters are plotted as a function of load in Figure 9, where crack length are plotted in normalized form as $K_c[H/E]^{1/2}c^{3/2}$. The data, which extend over 4 orders of magnitude in load, group nicely about a single line, implying that the assumed relation (Eqn.(8))works well for the cube corner indenter over a wide range of loads.

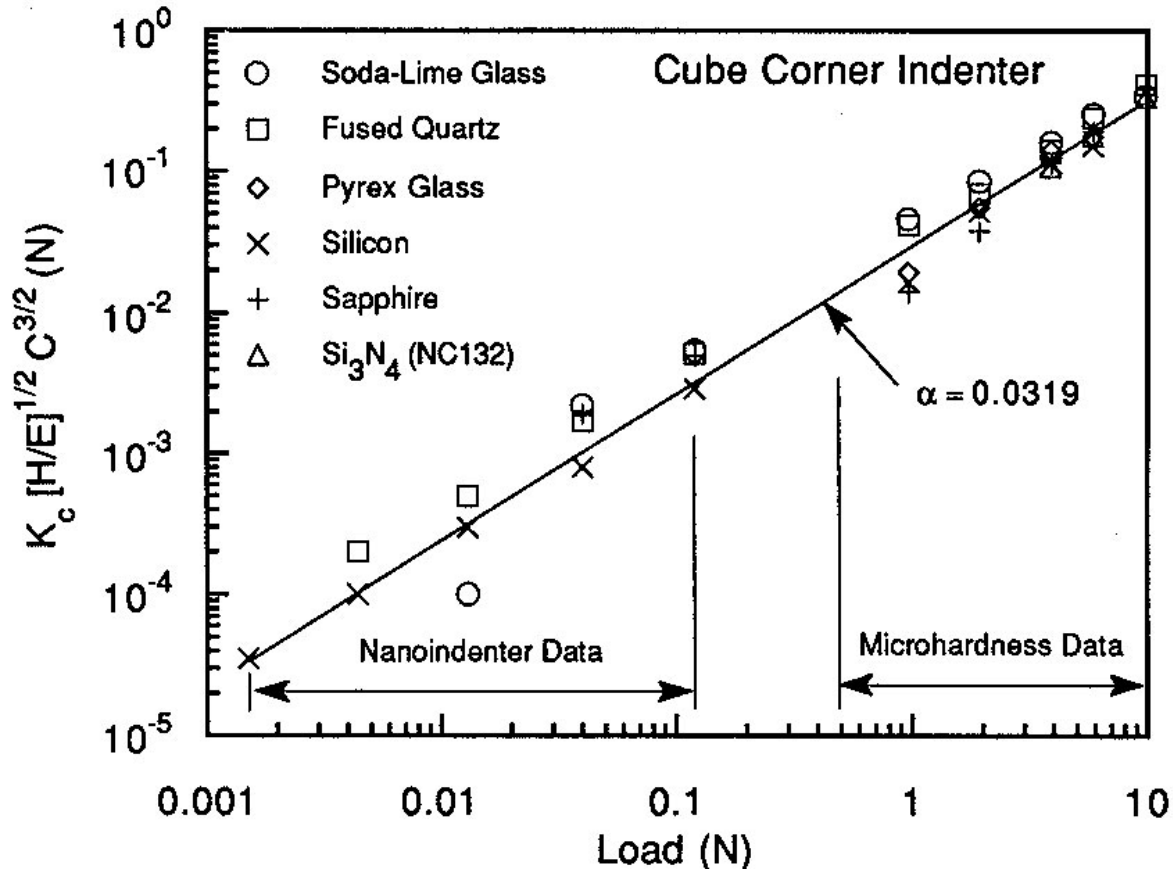


Figure 9. Plot of normalized crack length vs. applied load for the cube corner indenter. Data obtained in both microhardness and nanoindentation tests. [4]

APPLICATION TO OSG LOW-K THIN FILM

As semiconductor industry moving to Cu/low-K interconnects, the mechanical prosperities of OSG low-k material and how it survive a litany of processing steps that include dual-damascene lithography, etching, stripping and cleaning processes, CMP, and device packaging become important. A series of study on indentation fracture toughness of CVD OSG low-k thin film has been conduct in Gerberich group in University of Minnesota and Motorola [5][6][7][8][9].

Figure 10 represents three different scenarios one may observe using pyramid indentation. Fig. 10a is the desired configuration for radial cracks emanating from the corners of an indent. Due to the high shear stresses induced by the indenter pyramid edges subsurface delamination cracks are also observed for some indents (Fig. 10b and c).

As we see in Figure 11, the crack length c is much larger than the film thickness. Eqn.(10) should not be directly applied in the case of a thin film, since typically the crack shape is no longer halfpenny shape. An appropriate model should account for at least the film thickness and stress, and, preferably for the film porosity.

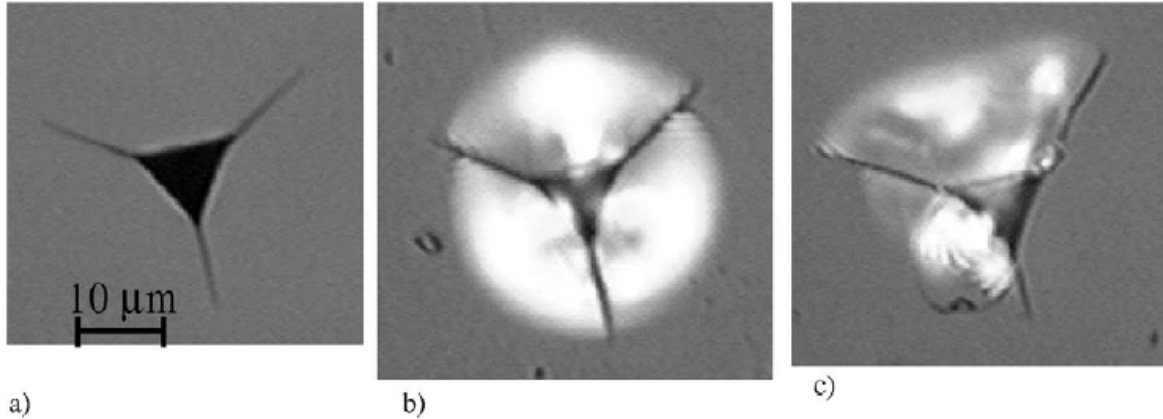


Figure 10. Optical micrographs of cube-corner indentation-induced fracture in fused silica: (a) radial cracks; (b) radial as well as symmetric sub-surface cracks; (c) radial and asymmetric sub-surface cracks. [9]

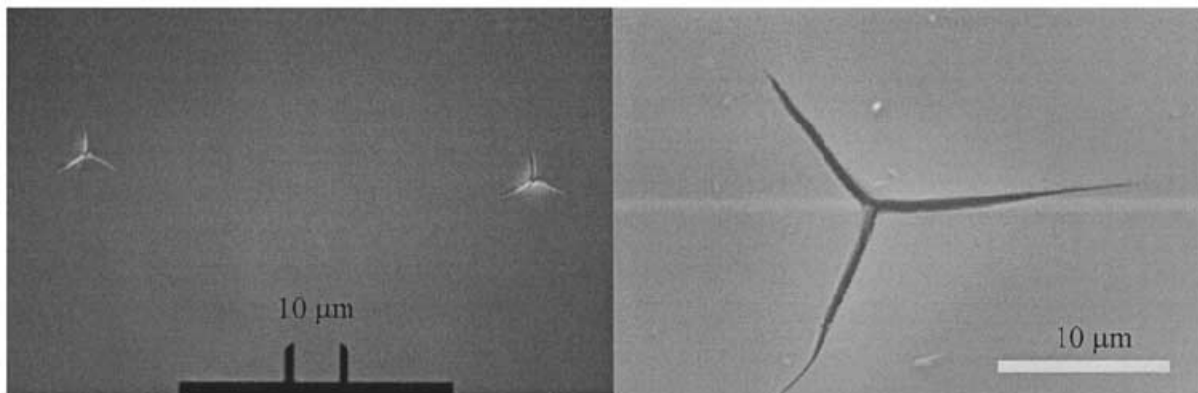


Figure 11. Optical and SEM image of cube-corner indentation-induced fracture in a 1 μm thick OSG low-K dielectric film.

Still, a plot of the maximum indentation load as a function of the crack length to the $3/2$ power, $c^{3/2}$ demonstrates a fairly linear relationship (Figure 12(a)). So as a first order approximation, Eqn. (10) can be used to estimate the low-K films fracture toughness (Figure 12(b)). Using this method the low-K dielectric films fracture toughness was estimated to range from 0.01 to 0.05 $\text{MPa}\cdot\text{m}^{1/2}$ [8].

Indentation fracture toughness measurement can also be made by the superlayer indentation test and cracking at the relief of residual stress at a critical film thickness. [7]

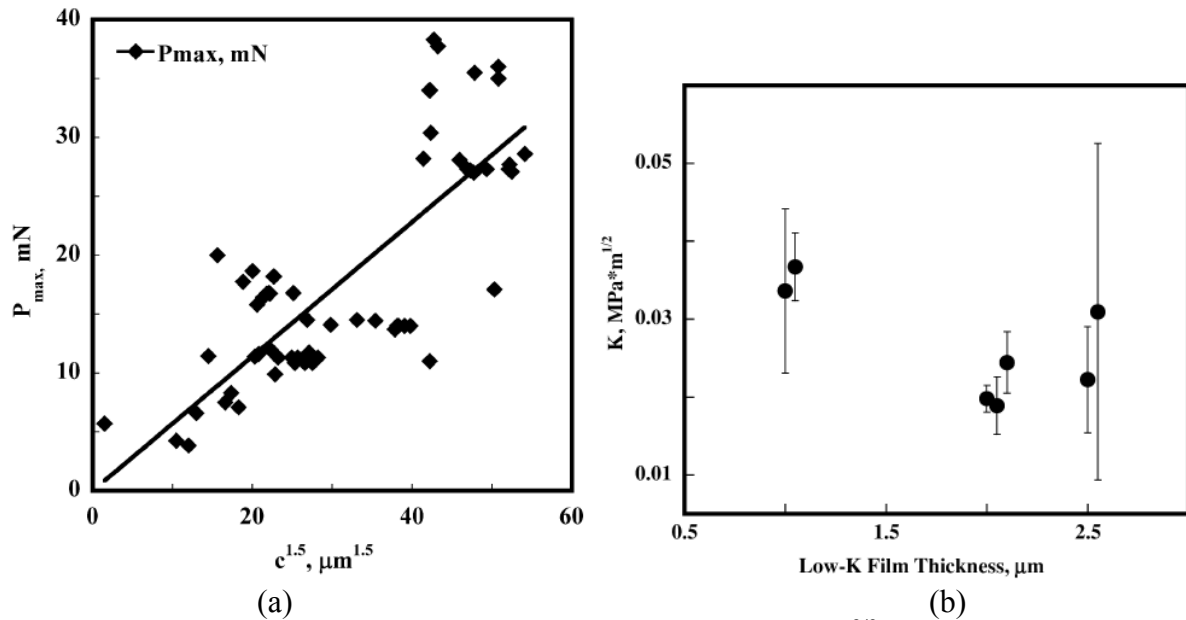


Figure 12. (a) Maximum indentation load P_{\max} as a function of $c^{3/2}$ [9]. (b) Measured low-K film toughness compared to the K value just due to the low-K film residual stress [7].

SUMMARY

Nanoindentation is a powerful technique that can be applied in modern microelectronics for measuring thin film mechanical properties. While measuring elastic and plastic properties with nanoindentation is almost routine, fracture toughness measurements are still in the development stage. Theoretical explanations, including analytical or FEM simulation solutions, of thin film indentation fracture are needed for the measurement of fracture toughness of thin films.

ACKNOWLEDGMENTS

This term paper is part of fulfillment of course EM 388F taught by Dr. Rui Huang at University of Texas at Austin. Special thanks to Prof. Rui Huang and classmates.

REFERENCES

1. M. F. Doerner and W. D. Nix, A Method for Interpreting the Data from Depth-Sensing Indentation Instruments, *J. Mater. Res.* **1**, 601-609 (1986)
2. B. Lawn, R. Wilshaw, Indentation fracture: principles and applications, *J. Mater. Sci.* **10** (1975)
3. B. Lawn, *Fracture of Brittle Solids* (second edition), Cambridge University Press, pp.249-306, (1993)
4. G.M. Pharr, D.S. Harding, W.C. Oliver, Mechanical Properties and Deformation Behavior of Materials Having Ultra-Fine Microstructures, M. Nastasi et al. (eds.), Kluwer Academic Press, pp. 449-461, (1993)

5. I. S. Adhietty, J. B. Vella, Alex A. Volinsky, et al., Mechanical Properties, adhesion, and fracture toughness of low-k dielectric thin films for microelectronic applications, Mechanics and Materials Summer Conference, San Diego, June, 2001
6. J. B. Vella, I. S. Adhietty, K Junker, A. A. Volinsky, Mechanical properties and fracture toughness of organo-silicate glass (OSG) low-k dielectric thin films for microelectronic applications, International Journal of Fracture, 119/120, pp.487–499, (2003)
7. A. A. Volinsky, W. W. Gerberich, Nanoindentation techniques for assessing mechanical reliability at the nanoscale, Microelectronic Engineering 69 (2003) 519–527
8. J. B. Vella, A. A. Volinsky, I.S. Adhietty, et al., Nanoindentation of Silicate Low-K Dielectric Thin Films, Mat. Res. Soc. Symp. Proc. Vol. 716 (2002)
9. A.A. Volinsky, J.B. Vella, and W.W. Gerberich, Fracture toughness, adhesion and mechanical properties of low-K dielectric thin films measured by nanoindentation, Thin Solid Films 429(1-2), 201–210, (2003)